



Chemotaxis of mesenchymal stem cells within 3D biomimetic scaffolds—a modeling approach

Christoph Landsberg^{a,b,*}, Florian Stenger^a, Andreas Deutsch^{b,d}, Michael Gelinsky^{c,d}, Angela Rösen-Wolff^{e,d}, Axel Voigt^a

^a Institute of Scientific Computing, Faculty of Mathematics and Natural Sciences, Technische Universität Dresden, Germany

^b Department for Innovative Methods of Computing, Center for Information Services and High Performance Computing (ZIH), Technische Universität Dresden, Germany

^c Max Bergmann Center of Biomaterials, Institute for Materials Science, Technische Universität Dresden, Germany

^d DFG Research Center and Cluster of Excellence for Regenerative Therapies Dresden (CRTD), Germany

^e Department of Pediatrics, University Clinics Carl Gustav Carus, Dresden, Germany

ARTICLE INFO

Article history:

Accepted 25 October 2010

Keywords:

Bone healing
Tissue engineering
Chemotaxis
Bulk/surface coupling
Adaptive finite elements

ABSTRACT

Bone tissue engineering is a promising strategy to repair local defects by implanting biodegradable scaffolds which undergo remodeling and are replaced completely by autologous bone tissue. Here, we consider a Keller–Segel model to describe the chemotaxis of bone marrow-derived mesenchymal stem cells (BMSCs) into a mineralized collagen scaffold. Following recent experimental results in bone healing, demonstrating that a sub-population of BMSCs can be guided into 3D scaffolds by gradients of signaling molecules such as SDF-1 α , we consider a population of BMSCs on the surface of the pore structure of the scaffold and the chemoattractant SDF-1 α within the pores. The resulting model is a coupled bulk/surface model which we reformulate following a diffuse-interface approach in which the geometry is implicitly described using a phase-field function. We explain how to obtain such an implicit representation and present numerical results on μ CT-data for real scaffolds, assuming a diffusion of SDF-1 α being coupled to diffusion and chemotaxis of the cells towards SDF-1 α . We observe a slowing-down of BMSC ingrowth after the scaffold becomes saturated with SDF-1 α , suggesting that a slow release of SDF-1 α avoiding an early saturation is required to enable a complete colonization of the scaffold. The validation of our results is possible via SDF-1 α release from injectible carrier materials, and an adaption of our model to similar coupled bulk/surface problems such as remodeling processes seems attractive.

© 2010 Elsevier Ltd. All rights reserved.

1. Introduction

Bone tissue is known to exhibit a great potential for self-healing, which originates from the lifelong and continuous process of remodeling of the bone matrix. Therefore, bone fractures mostly heal spontaneously if stabilized sufficiently. In most cases an implantation of cell-free biomaterials, e.g. calcium phosphate cements or porous ceramics, leads to complete healing unless the bone defect is too extended. In contrast, large defects, as for instance those in systemically diseased (e.g. osteoporotic) bone or tissue after radiotherapy, often do not heal by themselves. In such cases, the utilization of tissue engineered constructs, e.g. degradable scaffolds, seeded with autologous bone or stem cells, can improve healing and remodeling significantly (Gelinsky et al., 2010; Meyer and Wiesmann, 2006; Drosse et al., 2008). Today, living bone-like cell-matrix constructs can be generated in cubic

centimeter scale and be kept alive outside the body with the help of perfusion cell culture systems for weeks. Unfortunately, after implantation into the defect site most of the cells located inside of the porous scaffold die within a few hours because of insufficient oxygen and nutrient supply (Lode et al., 2008; Volkmer et al., 2008; Zhou et al., 2006).

Ingrowth of new blood capillaries into the scaffold, a process referred to as *vascularization*, takes too long for the cells to survive (Kanczler and Oreffo, 2008). In this respect, the classical tissue engineering concept fails just where it would be of highest importance: for healing of large bone defects. Many researchers therefore have started to investigate the generation of a prevascularized, artificial bone tissue. Another option for overcoming this problem is the so-called *in situ tissue engineering* approach (Mishima and Lotz, 2008; Otsuru et al., 2008), which has sometimes misleadingly been termed *in vivo* tissue engineering. In our approach, cell-free scaffolds are implanted into the defect and functionalized in such a manner that the formation of concentration gradients of chemoattractive substances leads to active migration of the cells necessary for the healing process (e.g. mesenchymal stem cells, in the case of a bone defect). The cells migrate as deep into the porous

* Corresponding author. Institut für Wissenschaftliches Rechnen, FR Mathematik, Technische Universität Dresden, Zellescher Weg 12–14, D-01062 Dresden, Germany. Tel.: +49 351 463 35493; fax: +49 351 463 37096.

E-mail address: Christoph.Landsberg@tu-dresden.de (C. Landsberg).

scaffold material as they are sufficiently supplied with oxygen and simultaneously secrete factors which stimulate the formation and ingrowth of new blood capillaries. Therefore, the healing process should be significantly accelerated while avoiding undersupply of cells in a pre-seeded scaffold, as occurs in many currently proposed tissue engineering therapies.

The homing of hematopoietic stem cells strongly depends on the interaction of stromal cell-derived factor 1α (SDF- 1α) and its receptor CXCR4. CXCR4 expressing cells migrate effectively in the direction of SDF- 1α gradients (Burger et al., 2003). Because a sub-population of mesenchymal stem cells expresses CXCR4, this population can be attracted by SDF- 1α (Otsuru et al., 2008). This interaction can be utilized to attract human mesenchymal stem cells as a subset of BMSCs into a porous three-dimensional (3D) scaffold, consisting of mineralized collagen type I (Thieme et al., 2009). The scaffold mimics the composition and ultrastructure of the extracellular matrix of bone and shows an interconnecting porosity which is a prerequisite for cellular ingrowth. Fig. 1(a) shows the material used for cell migration experiments and modeling: a porous biomimetic scaffold made of mineralized collagen, seeded with cells of a pre-osteoblastic line (ST-2).

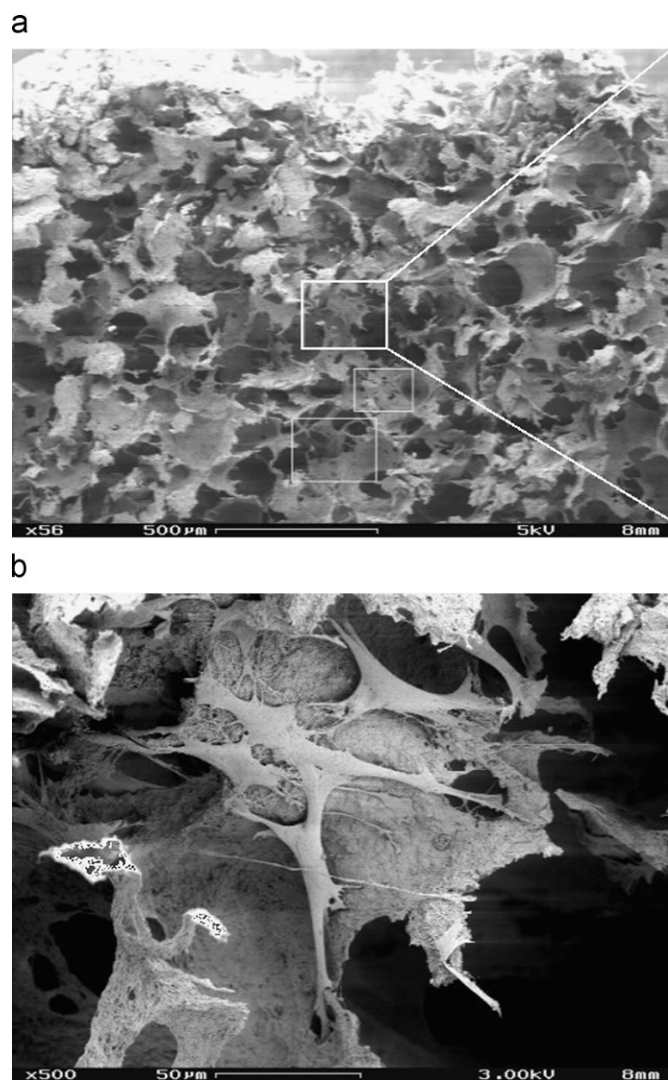


Fig. 1. Scanning electron micrographs of longitudinal sections of a porous mineralized collagen scaffold, seeded with osteoblast-like cells (murine cell line ST-2), used for cell migration experiments and modeling. (a) $200\times$ enlarged (b) sectional view, enlarging the $200\times$ image by a factor of 2.5 to a $500\times$ enlargement of approximately $250\times 200\mu\text{m}$. Kindly provided by Dr. Anne Bernhardt.

Fig. 1(b) shows that the cells attach and spread on the material which is a precondition for the colonization of the scaffold.

1.1. Modeling requirements

We consider a modeling approach to aid the understanding of the colonization inside the 3D scaffold. A detailed understanding of SDF- 1α directed invasion of internal compartments of the 3D scaffold to ensure a complete colonization by BMSCs is essential for the success of the *in situ tissue engineering* approach. In order to describe this approach mathematically, we have adapted an existing chemotaxis model and combined it with current numerical technologies. We consider a modified Keller–Segel model to simulate the chemotaxis of BMSCs into such scaffolds and to account for the porosity of the scaffold and the transport of cells along the scaffold surface. We also use a recent approach (Rätz and Voigt, 2006; Li et al., 2009) to efficiently solve partial differential equations (PDEs) on surfaces and in complex bulk domains, respectively. In this approach, the originally complicated scaffold geometry is embedded in a simple box, consisting of tetrahedra with identical shape. An *implicit* description of the complicated original geometry, i.e. a geometry representation without the need of *explicit* tracking of boundary geometries or topology information, is achieved in this approach by mapping numerical values of a continuous function termed *phase-field function* (PFF) to each grid point.

This function distributes distance and material information to the grid points and avoids sharp transitions between the material values of two neighbouring grid points, which would cause numerical problems. Where such sharp transitions still occur, the function can be used to refine the new geometry locally and subdivide the existing tetrahedra in an organized way. The original PDEs of interest are modified with the help of the PFF in order to calculate the solution of the new system of PDEs on the refined simple grid (Li et al., 2009).

We introduce the modified chemotaxis model and its numerical treatment. We will then discuss the technical issues of creating an appropriate representation of the μCT -data of the 3D scaffold suitable for a numerical simulation.

2. Materials and methods

2.1. Chemotaxis model

Mathematical modeling of chemotaxis, that is the movement of biological cells or organisms in response to chemical gradients, has developed into a large and diverse discipline (Othmer and Stevens, 1997; Hillen and Painter, 2009). The Keller–Segel model of chemotaxis (Keller and Segel, 1970, 1971a, b) has provided the basis for much of this work, describing the behaviour of a cell population u under the influence of a chemical v . One of its properties, the ability to display *auto-aggregation*, is a key mechanism for self-organization of biological systems. In classical settings of the Keller–Segel model in two (2D) or three (3D) dimensions (Horstmann, 2003, 2004), the solution can *blow-up*, i.e. the numerical values can grow without limitation in finite time (Velázquez, 2002). Biologically, this is equivalent to an overcrowding of cells in a limited spatial area, which is an unrealistic scenario resulting from the model assumption that cells are represented as single points without competition between each other for space or resources. A possibility to avoid such phenomena is the consideration of volume-filling models and cell density effects (Hillen and Painter, 2009). The properties of the various chemotaxis models in higher dimensions are less well understood and include *blow-up* and stable spherical aggregations (Wrzosek, 2004). We here modify the classical Keller–Segel model to describe the complex chemotaxis processes within the *in situ tissue engineering* approach. This requires a coupled bulk/surface model, as the cell population of BMSCs is modeled on the surface of the pore structure within the 3D scaffold, whereas the chemical SDF- 1α density has to be considered within the 3D pores of the scaffold.

We modify the classical Keller–Segel model (Keller and Segel, 1971a) to allow for transport of the BMSCs along the curved surface Γ . The density of the cells on Γ is denoted by u . SDF- 1α can diffuse through the pores of the scaffold Ω_0 . We denote the

density of SDF-1 α by v . Fig. 2 shows a 2D illustration of the domain. We consider $\partial_t u = \nabla_\Gamma \cdot (D_u \nabla_\Gamma u - \chi u \nabla_\Gamma v)$ on Γ (1)

$$\partial_t v = \nabla \cdot (D_v \nabla v) + g \quad \text{in } \Omega_0 \quad (2)$$

with ∇ the Nabla operator, D_u and D_v diffusion coefficients for u and v , χ the strength of the chemotactic transport and g a source term for SDF-1 α . As boundary condition for v we define

$$\frac{\partial v}{\partial \mathbf{n}} = 0 \quad \text{on } \partial\Omega_0, \quad (3)$$

stating zero flux in the direction of the unit normal vector \mathbf{n} , assuming that SDF-1 α does not diffuse into the solid material ($\Gamma \subset \partial\Omega_1$) and remains within the computational domain Ω . For u we specify $u = u_{\partial\Gamma}$ which models a source of BMSCs outside the domain. We further define initial conditions as $u(\cdot, 0) = u_0(\cdot)$ and $v(\cdot, 0) = v_0(\cdot)$ on Γ and Ω_0 , respectively. As in the classical Keller–Segel model, the cell flux on the right hand side of Eq. (1) comprises two counteracting phenomena: random motion of cells described by Fick’s law and cell movement in the direction of the gradient of the chemoattractant v . Only the operators are different as surface operators have to be considered. ∇_Γ denotes the surface gradient and $\nabla_\Gamma \cdot$ the surface divergence. Here, we neglect any influence of the cells u on the chemoattractant v as the effect is assumed to be very small.

The system of equations that we consider defines a coupled bulk/surface system for u and v , for which a classical approach will lead to severe problems concerning mesh generation. We will here concentrate on a more elegant way of using an implicit description of the geometry. Using the approach of Rätz and Voigt (2006), we can reformulate Eq. (1) into

$$B(\phi)\partial_t u = \nabla \cdot (D_u B(\phi)\nabla u - \chi u B(\phi)\nabla v) \quad \text{in } \Omega \quad (4)$$

where now u and v denote extended variables into Ω and $B(\phi) \approx \phi^2(1-\phi)^2$ is an approximation of a surface delta-function for Γ , with ϕ a phase-field variable defined through

$$\phi = \frac{1}{2} \tanh\left(1 - \frac{3r}{\varepsilon}\right) \quad (5)$$

with r a signed-distance representation of Γ and ε a small parameter determining the length scale on which the surface is smeared out. The phase-field function is essentially 1 in the pores of the scaffold and 0 in the solid part. In a similar way we can reformulate Eqs. (2) and (3) using the approach in Li et al. (2009) into

$$\phi\partial_t v = \nabla \cdot (D_v \phi \nabla v) + \phi g \quad \text{in } \Omega \quad (6)$$

As boundary conditions for u and v on $\partial\Omega$ we define

$$u = u_{\partial\Omega} \quad \text{on } \partial\Omega \quad (7)$$

$$\frac{\partial v}{\partial \mathbf{n}} = 0 \quad \text{on } \partial\Omega \quad (8)$$

respectively. As initial conditions we use the extended functions u_0 and v_0 . The resulting system is a coupled system of bulk equations in a regular domain which can be solved using standard approaches. It can be shown by matched asymptotic analysis that Eqs. (4) and (6) converge for $\varepsilon \rightarrow 0$ to Eqs. (1)–(3).

Our numerical treatment essentially follows the discretization approach in Saito (2007) for a classical Keller–Segel model. We consider the following discrete

formulation for the finite element functions u_h, v_h and ϕ_h with n indicating the time step:

$$\int_\Omega B(\phi_h) \frac{u_h^{n+1} - u_h^n}{\tau^n} \eta \, dx = - \int_\Omega D_u B(\phi_h) \nabla u_h^{n+1} \cdot \nabla \eta \, dx + \int_\Omega \chi u_h^{n+1} B(\phi_h) \nabla v_h^{n+1} \cdot \nabla \eta \, dx$$

with the Dirichlet boundary condition incorporated into the test functions η . The second equation decouples and reads

$$\int_\Omega \phi_h \frac{v_h^{n+1} - v_h^n}{\tau^n} \eta \, dx = - \int_\Omega D_v \phi_h \nabla v_h^{n+1} \cdot \nabla \eta \, dx + \int_\Omega \phi_h g \eta \, dx$$

Both equations are solved iteratively, starting with the second one. For this purpose, piecewise linear finite elements within the adaptive finite element toolbox AMDiS (Vey and Voigt, 2007) and BiCGStab(l) are used for solving the resulting linear system.

2.2. Preparation of 3D mineralized collagen scaffolds

Mineralization and 3D sample preparation of scaffold structures is achieved in several steps in which collagen fibrils are simultaneously assembled and mineralized, as described previously (Bradt et al., 1999). The protocol involves the subsequent mixing of a collagen I solution with a calcium-containing buffer at acidic conditions, followed by adding of a phosphate buffer under pH-neutral conditions. After incubation steps at 298 Kelvin (K), freeze-drying introduces interconnective pores with an average pore diameter of approximately 100–150 μm into the scaffold.

2.3. CT input data

Measurements of micro-computed tomography (μCT) data have been performed at the BAMLine μCT facility at the synchrotron light resource BESSY II of the Federal Institute for Materials Research and Testing (BAM) in Berlin and have been provided by Ricardo Bernhardt, a member of the Institute of Biomaterial Science in Dresden. The original dataset was obtained by applying a synchrotron beam energy of 12 keV, an angle step of 0.125°, a pixel resolution at the detector of 3.6 μm , and with two aluminum beam filters of sizes 0.2 and 0.5 mm, respectively. The specimen has a diameter of 6 mm, out of which we selected a small portion for simulation which is 0.7 mm in diameter and has a cubic shape.

2.4. Computing resources

Simulations and geometry conversions of specimen data were performed on a Linux cluster, i.e. a synergistic coupling of several computers with a Linux operation system installed on each single computer (node). The linux cluster combines the computing resources of 8 AMD Opteron X85 dual core processors with clock rates of 2.6 GHz and a total amount of 32 gigabytes (GB) of random access memory (RAM), which has been required for the conversion of the large μCT datasets. A detailed description of the conversion of μCT data into structured data are following.

2.5. Visualization

Visualization of the simulation results was done with Kitware ParaView, version 3.8.0, release candidate 2 (RC2), using a blue-to-red colouring and surface rendering filters (e.g. level set representations of the scaffold), with blue representing the lower values and red representing the higher values.

2.6. Geometry representation

One requirement for this approach is the phase-field function ϕ_h , or alternatively the signed distance representation r of the geometry, which has to be computed within a preprocessing step to be discussed later on in this paper. We will use μCT data as the geometric base of the model and obtain the signed distance representation for Γ . The geometry is originally given as a stack of μCT images, which depicts a cuboidal fragment of the scaffold. Instead of a conventional two-mesh approach, we follow an alternative approach especially suited for complicated domains, i.e. the implicit characterization of the solid material’s surface by a function representing both topological and distance values, termed *signed distance function* (Osher and Fedkiw, 2003).

We require only a single mesh, which is composed of tetrahedral elements filling the whole cube, including the interspaces within the solid material. The faces of the tetrahedra do not have to resemble the surface of the pore structure and may intersect it arbitrarily. The only requirement concerning the alignment of elements is that their size has to be small enough to ensure that we have a multitude of mesh-nodes in the immediate vicinity of the surface. The tetrahedra may get bigger with growing distance from the surface of the solid material. Fig. 3(a) shows the mineralized collagen scaffold from μCT data, Fig. 3(b) an explicit surface mesh of

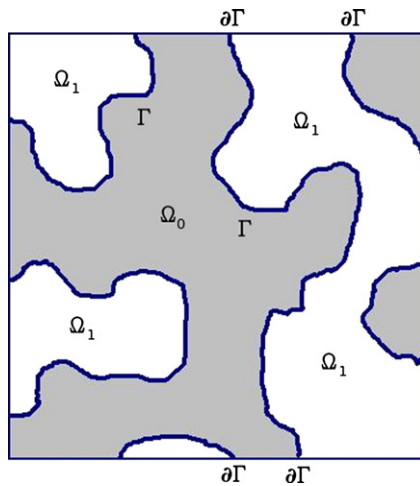


Fig. 2. Schematic representation of the domains of computation as an imaginative cut through a subregion of the mineralized collagen scaffold. Γ represents the surface of the mineralized collagen, (Ω_0) the inner space where the chemoattractant diffuses, and (Ω_1) the scaffold material. $\partial\Gamma$ corresponds to the boundary of Γ (in the 2D picture only points). The whole domain Ω consists of Ω_i , $i=0, 1$ and Γ .

a part of Fig. 3(a) and Fig. 3(c) shows the implicit volume mesh, which is adaptively refined along the surface of the pore structure.

Our tool, *meshconv*, uses a surface mesh as input. Since we initially have a stack of images, we need to generate a surface mesh with a different tool. Triangulation of surfaces is supported by many programs dealing with geometries, such as CAD-tools and computational geometry libraries, but the resulting mesh quality, while perfect for visualization, is usually insufficient for simulation software. ImageJ, a free image-processing software, which we use for this purpose, is no exception (Abramoff et al., 2004). However, our approach to calculate the implicit mesh allows the use of any surface mesh, as long as the surface is approximated well enough. The intermediate step involving a surface mesh is only one way of accomplishing this task. A potentially faster and less memory consuming approach is to directly refine the implicit mesh based on the μ CT images and to calculate the signed distances on the fly. We are currently working on an implementation.

3. Results

The goal of our modeling approach is to elucidate ways to ensure a complete invasion of the scaffold by BMSCs. The resulting model is a coupled bulk/surface model which has to be solved within the complex geometry of the scaffold. Using a diffuse-interface approach the model can be reformulated with the geometry implicitity described. The resulting system is solved on real geometries obtained from μ CT data of the scaffold.

Fig. 4 demonstrates the results for the signal concentrations (a1–d1) and cell densities (a2–d2), which are shown as pairs for each timestep, arranged in columns. At $t=0$, the signal concentration is initially restricted to a small spherical reservoir (data not shown) which subsequently spreads within the pores of the scaffold, as observed in timesteps $t=0.01$ – 0.2 s. During these timesteps, the corresponding cell density increases steadily, until the differences in the spatial distribution of SDF-1 α are significantly low. Both the SDF-1 α concentration differences and the cell density differences are simultaneously decreasing with time. This observation is consistent to the model equations, in which a flow term in the direction of the concentration gradient of the chemoattractant is used to represent chemotaxis of the cells (i.e. the second term of Eq. (1), which implies that this flow term becomes negligible for equally distributed concentrations of SDF-1 α).

For the modified Keller–Segel model (7)–(1) we calculate a series of timesteps for the coupled states of SDF-1 α and cell density distributions. We use a cubic section of the original scaffold specimen and visualize the simulation results on only one half of this cube, in order to show the source of SDF-1 α , placed in the center of the cubic section, being a subset of the original scaffold geometry which was obtained from the μ CT data.

4. Discussion

An important prerequisite for the simulations were the technical means for the geometric representations of original μ CT data. For generating implicit geometries as described above, and in order to handle large datasets, we therefore developed *meshconv*, a

mesh-conversion and -transformation tool that is distributed with our finite element software AMDiS, which is a toolbox for the solution of PDEs (Vey and Voigt, 2007). Meshconv takes a triangular surface mesh as input and generates the desired volumetric mesh and signed distance function in two steps. In the first step, a basic cuboidal mesh built of only six elements is refined until the desired number of nodes in close vicinity of the surface is reached. Refinement means that any tetrahedron intersecting the surface is split into two tetrahedra which may enforce splitting of neighbouring tetrahedra in order to meet the strict requirements of the simulation software. In the second step, each node of the mesh (i.e. each vertex of a tetrahedron) is assigned a real number specifying its distance from the surface, either with a positive sign if outside the solid material or with a negative sign to indicate it is inside the solid material.

The results show the feasibility of the computational approach to solve such bulk/surface problems on complex geometries. Other scenarios for the placing and distribution of initial chemoattractant sources may be regarded as a useful preparation for further experiments, and a molecular characterization of cellular signaling and signal uptake kinetics would enable the identification of unknown model parameters, such as the chemotactic sensitivity profile or growth dynamics and its influence on the colonization success. Improvements from the mathematical point of view consider the use of high-performance-computing (HPC) to allow simulations on larger parts of the scaffold and the use of more realistic parameters to allow for quantitative experimental validation and refinements of the chemotaxis model, as currently the available memory of the computer limits the size of scaffold region which can be geometrically represented.

HPC strategies which address this question are currently tested and further developed. In our case, the main idea to reduce the complexity of the μ CT datasets by decomposing the scaffold geometry representation, i.e. the tetrahedra-based embedding grid and associated data, into smaller non-overlapping datasets which can be handled by parallel computers or networks of computers.

Interestingly, the simulation results suggest the existence of small regions without SDF-1 α density, i.e. $u=0$, remaining within the scaffold, see the upper left corner of the images depicted in Fig. 4(a1–d1). This spot corresponds to a physically unlinked region contained in the scaffold geometry and may serve as an intrinsic control for the effectiveness of the computational approach.

In order to validate our simulations, materials like injectible hydrogels embedding signaling molecules, in our case SDF-1 α , can be applied and are being tested in ongoing experiments. These experiments improve earlier methods where the release of the signaling molecule was solely determined by the size of the signaling molecule and could not be controlled (Lode et al., 2008). The results of the earlier experiment are consistent with our observation, as they observe a limited ingrowth of cells in case of rapidly diffusing SDF-1 α . An inducible or fine-tuned diffusion of signaling molecules by chemical modifications of the carrier material would enable a more detailed validation of our model and offers a possibility to test

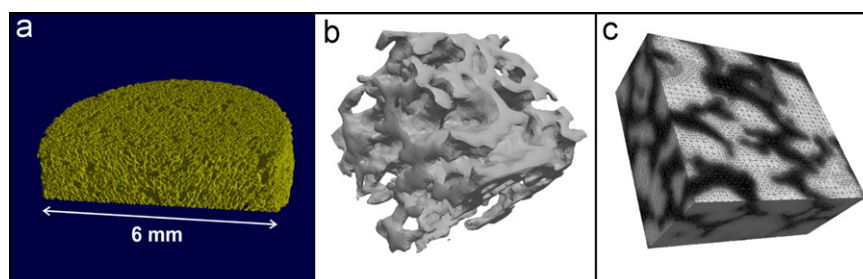


Fig. 3. (a) Visualization of SR μ CT data for a mineralized collagen I scaffold specimen. This image was taken from Gelinsky (2009) with permission of the publisher; an additional scalebar was introduced. (b) Explicit surface mesh of a part of the scaffold. (c) Implicit volumetric mesh of Ω which is adaptively refined along Γ .

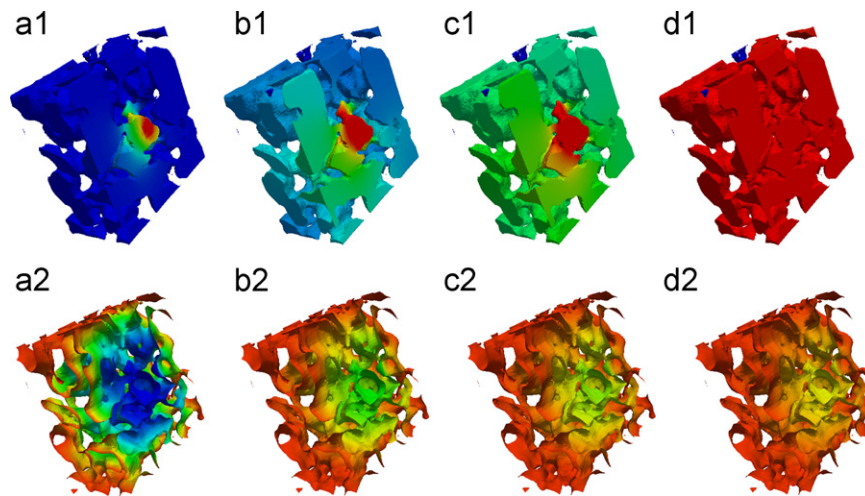


Fig. 4. Simulation results for the ingrowth of cells into a portion of scaffold (visualized on one-half of the cubic computational domain Ω). Images are organized in columns, representing an individual timestep of SDF-1 α diffusion and the density of BMSCs, which form corresponding pairs a1:a2, b1:b2, c1:c2 and d1:d2, respectively, each pair belonging to the same time point. *First row:* Diffusion of SDF-1 α through the pores of the scaffold, represented by Ω_0 , and being evaluated at 0.01, 0.1, 0.2 and 0.5 s, respectively, shown from left to right; the diffuse interface width used was $\varepsilon_D = 0.001$. A spherical reservoir of SDF-1 α of radius $R = 0.05$ is placed into the center of the cube ($x=y=z=0.5$), constantly providing SDF-1 α ; the initial SDF-1 α concentration is homogeneous with $v_{0,s} = 10.0$ within the sphere (indicated by red), and zero outside this region (indicated by blue). The initial state is not depicted. *Second row:* Cell densities for BMSCs at corresponding timesteps are shown, with a cell-free scaffold ($u_0 = 0$) as a starting condition (indicated by blue); cell density is introduced into the computational domain via Dirichlet boundary conditions for $\partial\Omega_0$, with $u_{\varepsilon\Omega} = 1$ (indicated by red); in this case, the diffuse interface width is $\varepsilon_D = 0.05$. Model parameters are $D_u = 0.5$, $D_v = 5.0$, $\chi = 0.5$ and $g = 10$ (within the mentioned spherical region, i.e. providing a constant source of SDF-1 α). A total of 4,774,702 gridpoints have been used to define 27,416,024 tetrahedral elements. The mesh is adaptively refined at the surface Γ with approximately four and eight grid points across the diffuse interface width ε , for SDF-1 α and BMSCs, respectively. Time is discretized with steps of $\tau = 0.0001$ s. Visualization was done with ParaView 3.8.0 RC2. (For interpretation of the references to colour in this figure legend, the reader is referred to the web version of this article.)

hypotheses about the growth and movement characteristics of the cells, which we currently simplify with constant parameter values.

Synchronizing the timescales of the simulations with existing experimental data may enable the validation of useful experiments to elucidate mechanistic details of the cell migration. In order to achieve this goal, a series of simulations could be done, and appropriate material parameters could be applied experimentally, in which the release kinetics of the signaling molecule would be varied to provoke cellular responses. The resulting cellular behaviour would assess the model and enable improvements and extensions of our model towards more realistic descriptions of BMSC movement through 3D environments.

Likewise, our simulations could be used to validate the feasibility of experimental hypotheses about such cellular movement characteristics. For the general case of arbitrary 3D scaffolds, microscopic techniques to observe living cells in non-transparent materials are not yet available, limiting the experimental feedback required to refine our model. Besides these limitations, our model can be adapted to a variety of problems, as bulk/surface phenomena which are abundant in nature. In the context of tissue engineering, additional physical aspects, such as adhesion of molecules or cells to the cell surface and interactions of different cell populations with each other, may be interesting options for further extensions and applications of our model.

A number of factors act as chemoattractants of mesenchymal stem cells, e.g. fibronectin, platelet derived growth factor (PDGF) and bone morphogenetic proteins 2 and 4 (BMP-2, -4) (Mishima and Lotz, 2008; Fiedler et al., 2002; Thibault et al., 2007), increasing the number of possible model variants for different combinations of signaling molecules, scaffold materials, and cell types, and enhancing the clinical potential for the *in situ tissue engineering* approach.

Conflict of interest statement

The authors declare that there is no conflict of interest related to this work.

Acknowledgements

We thank Dr. Anne Bernhardt for providing scanning electron micrographs, Dr. Anja Lode for cell culture studies, Dr. Jürgen Goebels and Dr. Heinrich Riesemeier for the acquisition of μ CT data of the scaffold specimen, Dr. Ricardo Bernhardt for providing preprocessed geometry data and for support with image processing, and Dr. Manfred Bobeth for insightful discussions. This study has been carried out as preparatory work for the newly established special research field SFB/TR 79 and is currently supported by the German Research Foundation (DFG) within the project Vo899/6-2.

References

- Abramoff, M., Magalhaes, P.J., Ram, S., 2004. Image processing with ImageJ. *Biophotonics International* 11, 36–43.
- Bradt, J., Mertig, M., Teresiak, A., Pompe, W., 1999. Biomimetic mineralization of collagen by combined fibril assembly and calcium phosphate formation. *Chemistry of Materials* 11, 2694–2701.
- Burger, J., Spoo, A., Dwenger, A., Burger, M., Behringer, D., 2003. CXCR4 chemokine receptors (CD184) and $\alpha 4 \beta 1$ integrins mediate spontaneous migration of human CD34+ progenitors and acute myeloid leukaemia cells beneath marrow stromal cells (pseudoemperipolesis). *British Journal of Haematology* 122, 579–589.
- Drosse, I., Volkmer, E., Capanna, R., Biase, P., Mutschler, W., Schieker, M., 2008. Tissue engineering for bone defect healing: an update on a multi-component approach. *Injury* 39, S9–S20.
- Fiedler, J., Röderer, G., Günther, K.P., Brenner, R.E., 2002. BMP-2, BMP-4, and PDGF-bb stimulate chemotactic migration of primary human mesenchymal progenitor cells. *Journal of Cellular Biochemistry* 87, 305–312.
- Gelinsky, M., 2009. Mineralised collagen as biomaterial and matrix for bone tissue engineering. In: *Fundamentals of Tissue Engineering and Regenerative Medicine* first ed. Springer, Heidelberg, Berlin, pp. 485–493.
- Gelinsky, M., Lode, A., Bernhardt, A., Rosen-Wolff, A., 2010. Stem cell engineering for regeneration of bone tissue. In: *Stem Cell Engineering* first ed. Springer, Heidelberg and Berlin, pp. 379–394.
- Hillen, T., Painter, K., 2009. A user's guide to PDE models for chemotaxis. *Journal of Mathematical Biology* 58, 183–217.
- Horstmann, D., 2003. From 1970 until present: the Keller–Segel model in chemotaxis and its consequences I. *Jahresbericht der Deutschen Mathematiker-Vereinigung* 105, 103–165.
- Horstmann, D., 2004. From 1970 until now: the Keller–Segel model in chemotaxis and its consequences II. *Jahresbericht der Deutschen Mathematiker-Vereinigung* 106, 51–69.

- Kanczler, J., Oreffo, R., 2008. Osteogenesis and angiogenesis: the potential for engineering bone. *European Cells and Materials* 15, 100–114.
- Keller, E., Segel, L., 1970. Initiation of slime mold aggregation viewed as an instability. *Journal of Theoretical Biology* 26, 399–415.
- Keller, E., Segel, L., 1971a. A model for chemotaxis. *Journal of Theoretical Biology* 30, 225–234.
- Keller, E., Segel, L., 1971b. Travelling bands of chemotactic bacteria: a theoretical analysis. *Journal of Theoretical Biology* 30, 235–248.
- Li, X., Lowengrub, J., Raetz, A., Voigt, A., 2009. Solving PDEs in complex geometries: a diffuse domain approach. *Communications in Mathematical Sciences* 7, 81–107.
- Lode, A., Bernhardt, A., Gelinsky, M., 2008. Cultivation of human bone marrow stromal cells on three-dimensional scaffolds of mineralized collagen: influence of seeding density on colonization, proliferation and osteogenic differentiation. *Journal of Tissue Engineering and Regenerative Medicine* 2, 400–407.
- Meyer, U., Wiesmann, H., 2006. *Bone and Cartilage Engineering*. Springer Verlag.
- Mishima, Y., Lotz, M., 2008. Chemotaxis of human articular chondrocytes and mesenchymal stem cells. *Journal of Orthopaedic Research* 26, 1407–1412.
- Osher, S., Fedkiw, R., 2003. *Level Set Methods and Dynamic Implicit Surfaces*. Springer Verlag.
- Othmer, H., Stevens, A., 1997. Aggregation, blowup and collapse: the ABC's of taxis in reinforced random walks. *SIAM Journal on Applied Mathematics* 57, 1044–1081.
- Otsuru, S., Tamai, K., Yamazaki, T., Yoshikawa, H., Kaneda, Y., 2008. Circulating bone marrow-derived osteoblast progenitor cells are recruited to the bone-forming site by the CXCR4/stromal cell-derived factor-1 pathway. *Stem Cells* 26, 223–234.
- Rätz, A., Voigt, A., 2006. PDE's on surfaces—a diffuse interface approach. *Communications in Mathematical Sciences* 4, 575–590.
- Saito, N., 2007. Conservative upwind finite-element method for a simplified Keller–Segel system modelling chemotaxis. *IMA Journal of Numerical Analysis* 27, 332–365.
- Thibault, M., Hoemann, C., Buschmann, M., 2007. Fibronectin, vitronectin, and collagen I induce chemotaxis and haptotaxis of human and rabbit mesenchymal stem cells in a standardized transmembrane assay. *Stem Cells and Development* 16, 489–502.
- Thieme, S., Ryser, M., Gentsch, M., Brenner, S., Stiehler, M., Rölfing, J., Gelinsky, M., Rösen-Wolff, A., 2009. Stromal cell-derived factor-1 α —directed chemoattraction of transiently CXCR4-overexpressing bone marrow stromal cells into functionalized three-dimensional biomimetic scaffolds. *Tissue Engineering Part C: Methods* 15, 687–696.
- Velázquez, J., 2002. Stability of some mechanisms of chemotactic aggregation. *SIAM Journal on Applied Mathematics* 62, 1581–1633.
- Vey, S., Voigt, A., 2007. AMDiS: adaptive multidimensional simulations. *Computing and Visualization in Science* 10, 57–67.
- Volkmer, E., Drosse, I., Otto, S., Stangelmayer, A., Stengele, M., Kallukalam, B., Mutschler, W., Schieker, M., 2008. Hypoxia in static and dynamic 3D culture systems for tissue engineering of bone. *Tissue Engineering Part A* 14, 1331–1340.
- Wrzosek, D., 2004. Global attractor for a chemotaxis model with prevention of overcrowding. *Nonlinear Analysis* 59, 1293–1310.
- Zhou, Y., Sae-Lim, V., Chou, A., Huttmacher, D.W., Lim, T., 2006. Does seeding density affect in vitro mineral nodules formation in novel composite scaffolds? *Journal of Biomedical Materials Research Part A* 78, 183–193.